CrossMark

Competitive influence of surface area and mesopore size on gas-sensing properties of SnO$_2$ hollow fibers

Jinjin Wu[1] · Dawen Zeng[2] · Shouqin Tian[3] · Keng Xu[2] · Daoguang Li[2] · Changsheng Xie[2]

Abstract In this work, the effects of surface area and mesopore size on gas-sensing properties of SnO$_2$ hollow microfibers assembled by nanocrystals were investigated. When the sintering time was increased from 2 to 24 h, the specific surface area (SSA) of SnO$_2$ microfibers decreased from 103.6 to 59.8 m^2 g^{-1}, whereas the mesopore diameter gradually increased from 2.8 to 10.9 nm. Interestingly, it was found that their gas-sensing properties to ppb-level formaldehyde were determined by both SSA and mesopore size. The gas response increased firstly and then decreased with decreasing SSA and increasing mesopore size and reached the maximum value when the sintering time was 11 h. When the sintering time was <11 h, mesopore size (<8.5 nm) dominated sensing behavior by controlling gas diffusion rate. Once the sintering time was more than 11 h, the decreased SSA (<70.8 m^2 g^{-1}) dominated sensing performance by influencing the surface reaction activity. Therefore, the competitive influence of surface area and mesopore size on gas-sensing properties of mesoporous SnO$_2$ microfibers was revealed. This work could provide a new understanding for microstructural design of the mesoporous gas-sensing metal oxide materials.

Introduction

Metal oxide semiconductor materials, such as WO$_3$, ZnO, SnO$_2$, and In$_2$O$_3$, have attracted considerable attention due to their unique properties and potential application in gas sensors [1–4]. With regard to WO$_3$, the interaction between its crystal structure and the gas molecules is of an intercalating nature, changes the band structure of WO$_3$, increases its conductivity, and can be used for sensing applications [5]. For SnO$_2$-based gas sensors, the sensing mechanism has been studied for decades, and the "oxygen ionosorption" theory is mostly accepted [6, 7]. This theory can be used to interpret the adsorption and the reaction of analyte gases with oxygen species adsorbed on the surface. Therefore, the gas-sensing process can be considered as a phenomenon in which gas diffusion and reaction are coupled together [8]. Considerable efforts are devoted to improving the sensing performance of metal oxide materials by adjusting microstructural properties, including surface area and mesopore size [9–11]. It is well known that larger surface area will enable more adsorption and reaction active sites, resulting in higher gas response [12–14].

The gas diffusion is an infrequently discussed yet important factor for sensing performance, and the defined mesopore size affects diffusion quite substantially [15]. In the mesoporous metal oxide materials whose pore diameter is in the range from 2 to 50 nm, the mean free path of a gas molecule is determined by the pore walls rather than by

✉ Dawen Zeng
dwzeng@hust.edu.cn

✉ Changsheng Xie
csxie@hust.edu.cn

[1] Analytical and Testing Center, Huazhong University of Science and Technology (HUST), No. 1037, Luoyu Road, Wuhan 430074, People's Republic of China

[2] State Key Laboratory of Materials Processing and Die & Mould Technology, Huazhong University of Science and Technology (HUST), No. 1037, Luoyu Road, Wuhan 430074, People's Republic of China

[3] State Key Laboratory of Silicate Materials for Architectures, Wuhan University of Technology, No. 122, Luoshi Road, Wuhan 430070, People's Republic of China

adjacent molecules, and thus the gas molecules are more likely to collide with the pore wall and then reacts with adsorbed oxygen species [7, 16]. Sakai described the dependence of gas response on mesopore sizes and channel depths successfully [17]. In this sense, for mesoporous gas sensors, the Knudsen diffusion plays a crucial role on the sensing performance. Compared with mesopores, macropores (diameter >50 nm) have less influence on the diffusion due to the fact that big pores allow the target gas to quickly diffuse in by molecular diffusion.

Conventionally, reducing grain size will on the one hand result in higher surface area, which may lead to high gas response by exposing more active adsorption and reaction site to gas molecules; on the other hand, smaller interparticle pores may be disadvantageous, an effect which may overcompensate the positive effect of grain size [7, 15]. This demonstrates that pore diameter and SSA are correlated in the porous metal oxide materials with potentially opposite impacts on the sensing performance. Recently, Tian has investigated the effects of pore diameter on gas-sensing properties of porous SnO_2 materials with different calcining temperatures and attributed the higher sensitivity of porous SnO_2 calcined at 800 °C to the larger pore diameter and the resultant effective surface area [18]. But another report has proved that the pore volume showed higher consistency with gas response rather than effective surface area [19]. Moreover, the grain growth has a profound effect in changing organized pore arrangement. When the pore diameter increased at elevated temperature, the diffusion rate changed correspondingly, and thus the sensing performance may be deteriorated [20]. Therefore, it remains a challenge to evaluate the effects of the two characteristics, surface area and mesopore diameter, on gas-sensing properties of metal oxide sensors systematically.

In order to investigate the variation of surface area and mesopore size of SnO_2, as well as their influence on the gas-sensing properties simultaneously, SnO_2 hollow fibers were prepared by sintering with different times from 2 to 24 h at 600 °C. The detailed characterizations showed that the mesopore diameter increased, whereas the SSA gradually decreased with increasing sintering time. Interestingly, we found that firstly the gas response increased with the mesopore diameter when the sintering time increased from 2 to 11 h, and then it decreased drastically when the sintering time kept on increasing. The competitive influence of surface area and mesopore size on gas-sensing properties of mesoporous SnO_2 hollow fibers was discussed qualitatively. Throughout the characterizations and the gas-sensing tests, it should be noted that the sensing performance is deemed to be a result of synergistic influence of surface area and mesopore size.

Experimentation

Materials and synthesis

All the chemical reagents were of analytical grade and utilized as purchased without further purification. The materials were prepared as follows. 0.3 g of $SnCl_2·2H_2O$ was added into 60 ml of pyridine, followed by stirring at room temperature until the $SnCl_2·2H_2O$ was dissolved completely. This solution was transferred into a 70-ml stainless steel Teflon-lined autoclave, and 0.25 g of absorbent cotton was dipped into the solution. Then the autoclave was tightened and heated up at 120 °C for 24 h in oven. When the autoclave cooled down to room temperature, the cotton–SnO_2 hybrid was took out and washed with copious ethanol and water. Then this hybrid was dried in air at 80 °C for 24 h. To remove the cotton and make the SnO_2 crystallize, this hybrid was sintered at 600 °C (heating rate was 3 °C min^{-1}) for 2, 6, 11, 17, and 24 h in a resistance-heated furnace, and the obtained products were denoted as Sn2h, Sn6h, Sn11h, Sn17h, and Sn24h, respectively.

Characterization

The X-ray diffraction (XRD) patterns were recorded on a Philips X'Pert diffractometer in the range from 20° to 80° using Cu Kα1 radiation ($\lambda = 1.5406$ Å). The nitrogen adsorption–desorption isotherms were measured by Quantachrome AUTOSORB-1 at 77 K, and the Brunauer–Emmett–Teller (BET) and Barrett–Joyner–Halenda (BJH) methods were used here to calculate the SSA and pore size distribution, respectively. Scanning electron microscopy (SEM) observations were conducted using an FEI Sirion 200 microscopy at an acceleration voltage of 10.0 kV. High-resolution transmission electron microscope (HRTEM) characterization was performed with an FEI Tecnai G220 microscope at 200 kV.

Sensor fabrication and measurement of gas-sensing properties

The sensors were fabricated as follows: the sintered SnO_2 fibers and a suitable amount of ethanol were mixed to form a paste. Then the paste was coated on the surface of alumina ceramic tubes, which had two Au electrodes and Pt wires at both ends. The coated ceramic tubes were sintered at 500 °C for 2 h. A small heating wire of Ni–Cr alloy was inserted through a ceramic tube when the ceramic tube was fixed on a 6-stitch substrate. In order to improve the long-term stability of the sensors, the sensor devices were aged at 320 °C for 5 days in air.

The gas-sensing properties were tested in a steel-made chamber through which a controlled atmosphere was allowed to flow. The electrical response of the sensor was measured with an automatic test system, controlled by personal computer [1]. The gas response was defined as the resistance ratio R_a/R_g, where R_a and R_g stand for the electrical resistance in dry air and in the tested gas, respectively. Our testing formaldehyde gas with different concentrations can be obtained by mixing dry air and formaldehyde specimen gas (120 ppm in N_2 without water vapor) which was purchased from Shanghai Weichuang Standard Gas Analytical Technology Co., Ltd., Shanghai, China.

Results and discussion

Structure and morphology

Figure 1 shows XRD patterns of cotton–Sn hybrid and sintered SnO_2 fibers. One peak was observed in the pattern of cotton–SnO_2 hybrid, which could be indexed to the characteristic (002) plane of the cotton fiber crystal phase [21]. No peak corresponding to tin-related compound was found, indicating that the state of tin was amorphous. The peak of cotton fibers disappeared in the patterns of sintered specimens, and many new diffraction peaks were observed. All these new peaks agreed well with the tetragonal structure in JCPDS 41-1445 (cassiterite), suggesting that the sintered specimens consisted of tetragonal SnO_2. This result indicated good crystallization of SnO_2 and complete decomposition of organic cotton [22]. Furthermore, the crystalline size of SnO_2 was calculated using Scherrer formula [23]:

$$D = 0.9\lambda/\beta\cos\theta, \qquad\qquad (i)$$

where θ is the Bragg angle, β the full width at half maxima, and $\lambda = 1.5406$ Å. The crystalline sizes of Sn2h, Sn6h, Sn11h, Sn17h, and Sn24h were 5.8, 6.6, 7.4, 9.7, and 11.3 nm, respectively. This result indicated that continuous sintering resulted in an increase in the grain size of SnO_2.

Figure 2a, b shows the SEM images of Sn2h and Sn24h, respectively. These two specimens were of the similar appearance which was a replica of cotton fiber. The diameter of the sintered fiber was estimated to be 5–10 μm, which was in line with our previous report [3]. As shown in the inset of Fig. 2a, the hole of SnO_2 hollow fibers was about 2 μm. The sintered fibers showed a little shrinkage, compared with the diameter (about 20 μm) of absorbent cotton [21]. To further observe the nanostructure of the fibers, HRTEM was carried out. Figure 2c, d, and e shows the HRTEM images of Sn2h, Sn11h, and Sn24h, respectively. These images demonstrated that the hollow fibers were of hierarchical nanostructure assembled by fine nanocrystals. As shown in Fig. 2c, the crystalline size of Sn2h was small and the pores (as denoted by the dashed line) were encapsulated by SnO_2 nanocrystals. When the sintering time was increased to 11 h, the crystalline size increased slightly and the pore diameter became larger than Sn2h, as shown in Fig. 2d. Eventually, the sintering time was increased to 24 h, SnO_2 crystals grew up, and the pore diameter kept on increasing, as shown in Fig. 2e. Interplanar distances of 0.34 nm corresponding to tetragonal (110) plane could be observed from the inset of Fig. 2d [24]. To investigate the variation of SnO_2 nanocrystals, we selected different HRTEM images of three specimens and measured the grain size of SnO_2 nanocrystals. Thus the dependence of SnO_2 grain size on sintering time is plotted in Fig. 2f. The grain sizes of Sn2h, Sn11h, and Sn24h were 6.9, 7.3, and 9.9 nm, respectively. The change of SnO_2 nanocrystals may put significant influence on the gas-sensing properties.

To further investigate the porous nanostructure of the sintered SnO_2 fibers, the nitrogen adsorption–desorption characterization was carried out. As shown in Fig. 3, the isotherms of Sn2h, Sn11h, and Sn24h were all characteristic of a type IV with a type H3 hysteresis loop, indicating that the materials had aggregates of platelike particles forming slitlike pores [18, 25]. As calculated by BET method, the SSA of the five specimens was 103.6, 82.8, 70.8, 68.3, and 59.8 m^2 g^{-1}. The SSA showed a decreased trend when sintering time increased gradually (as listed in Table 1). This variation could be ascribed to the growth of SnO_2 nanocrystals. The pore diameter distribution of the Sn2h, Sn11h, and Sn24h calculated by BJH method is shown in the inset of Fig. 3. The average pore diameters of the five specimens increased with increasing sintering time,
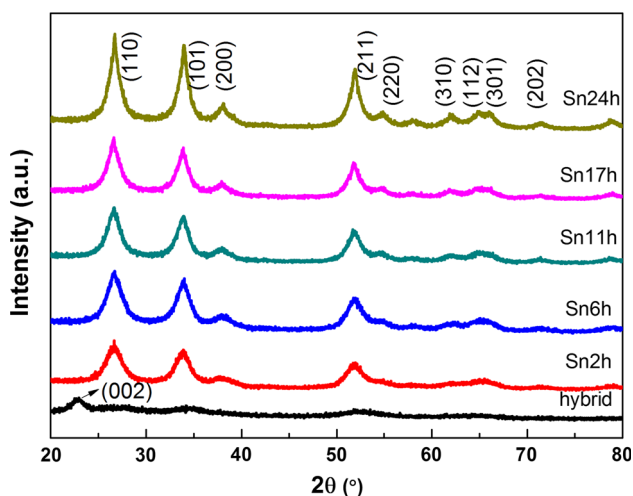

Fig. 1 XRD patterns of SnO_2–cotton hybrid and sintered SnO_2 microfibers

Fig. 2 The SEM images of Sn2h (**a**) and Sn24h (**b**) and the HRTEM images of Sn2h (**c**), Sn11h (**d**), and Sn24h (**e**), respectively. The inset of **a** and **d** shows the typical hollow structure of SnO$_2$ fibers and fine SnO$_2$ grains with (110) lattice plane, respectively. The grain sizes of Sn2h, Sn11h, and Sn24h collected from different HRTEM images are shown in (**f**)
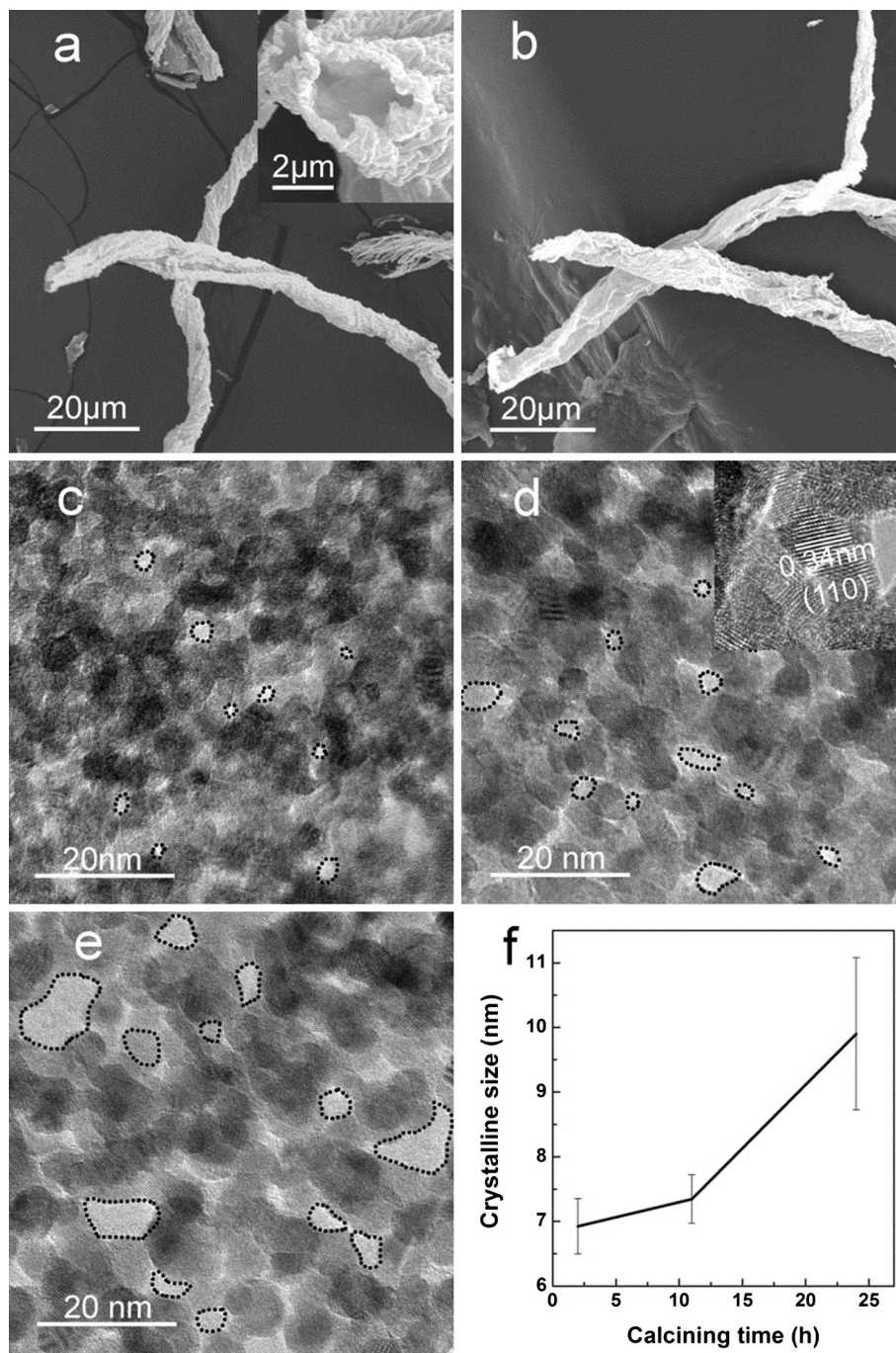
as listed in Table 1. The specimens showed large surface area and mesoporous nanostructure, and thus they were supposed to exhibit remarkable gas-sensing properties.

Gas-sensing properties

The gas-sensing tests were carried out to investigate the relationship between the gas-sensing properties of the specimens and their structural characteristics, SSA and pore diameter. Figure 4 shows the gas response of the

sensors based on sintered SnO$_2$ hollow microfibers to 300 ppb formaldehyde at operating temperature ranging from 120 to 320 °C. The result indicated that the response of the sensors were strongly dependent on operating temperature. The volcano-shaped temperature dependence of the response has been theoretically explained by surface reaction and gas diffusion kinetics [16, 26]. It was notable that Sn11h exhibited a higher gas response to formaldehyde compared with any other specimens. The response of Sn11h rose gradually with increasing operating

temperature and reached the maximum value (16.3–300 ppb formaldehyde) at 240 °C, and then it decreased drastically when the operating temperature kept on increasing. Sn6h, Sn17h, and Sn24h also showed their highest response at 240 °C. Sn2h showed a lower optimal operating temperature which could be ascribed to its higher surface activity due to its smallest grain size [26].

The response–recovery curves of the five specimens at 240 °C are shown in Fig. 5. It was found that all the five specimens exhibited good response–recovery characterizations at different concentrations. The response was reversible, and the response values of each specimen increased with increasing gas concentration. Among these specimens, Sn11h exhibited the highest gas response and its response was 6.1, 9.5, 16.3, and 19.6 to 50, 100, 300, and 500 ppb formaldehyde, respectively. It was found that the gas response firstly increased and then decreased with increasing sintering time, while the optimal gas response was shown in SnO_2 hollow fibers sintered for 11 h. Additionally, the base line of the sensors' resistance varied with sintering time. With increasing sintering time, the resistance of SnO_2 sensors increased gradually and Sn11h showed the highest resistance. However, the resistance augmented as the sintering time increased from 11 to 24 h.
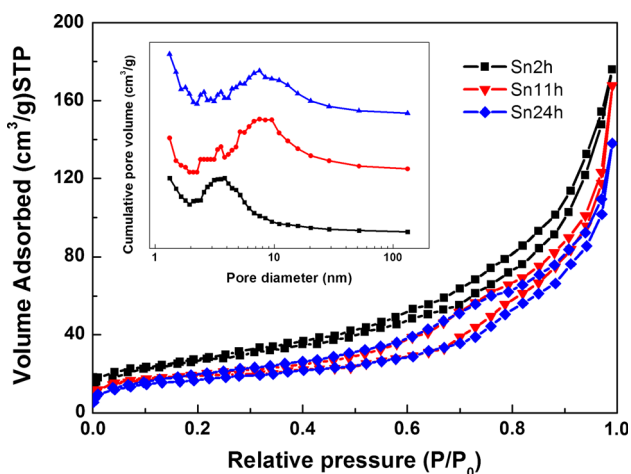
The mechanism for the enhanced gas response of Sn11h and variation of sensors' resistance were discussed in detail later.

The response and recovery times are key parameters to evaluate the performance of the metal oxide gas sensor. According to the date in the dynamic response–recovery
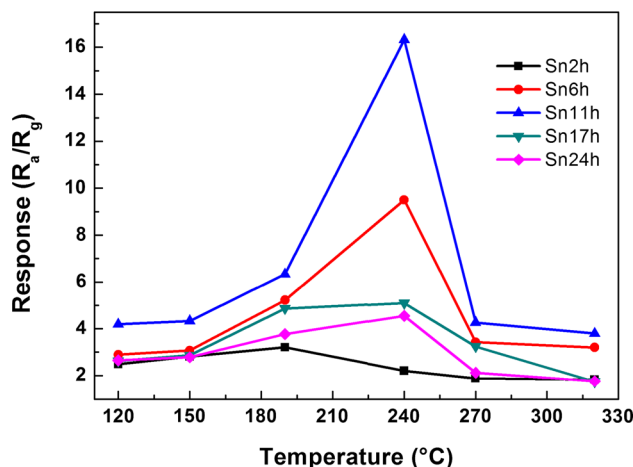

Fig. 4 Dependence of the gas response of the five specimens to 300 ppb formaldehyde on operating temperature
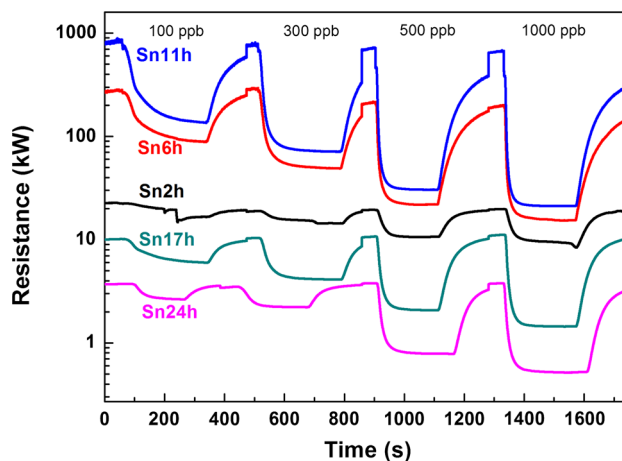

Fig. 3 Nitrogen adsorption–desorption isotherms of Sn2h, Sn11h, and Sn24h and their pore size distribution in the inset panel

Fig. 5 Dynamic response–recovery curves of the five specimens to formaldehyde gas with various concentrations at 240 °C

Table 1 The SSA, average pore diameter, and response and recovery time of the mesoporous SnO_2 specimens

Sintering time (h)	Specific surface area (m²/g)	Average pore diameter (nm)	Response time (s)	Recovery time (s)
2	103.6	2.8	54.8	81.8
6	82.8	5.6	42.6	70.5
11	70.8	8.5	36	48
17	68.3	8.5	41.2	62.5
24	59.8	10.9	66.4	132.1

test (as listed in Table 1), the response and recovery time of the five specimens to 300 ppb formaldehyde gas at an operating temperature 240 °C were prepared to investigate the influence of sintering time on the gas-sensing properties. The time taken by the sensor to achieve 90 % of the total resistance change is defined as the response time in the case of injecting the target gas in or the recovery time in the case of keeping the target gas out [27]. Both the response and recovery times of the five specimens, as shown in Table 1, firstly decreased and then increased with increasing sintering time at 240 °C. As plotted in Fig. 6, the sensor of Sn11h exhibited the shortest response (36 s) and recovery time (48 s) among the specimens. Therefore, the surface area of Sn11h cooperated with its relatively wide pore diameter to demonstrate the best gas permeability, which would change the response and recovery time essentially [27, 28]. Although the pore diameter of Sn24h was the widest among the specimens, the low surface reactivity of the larger grain size slowed down the reaction rate of analyte gas reacted on SnO$_2$ surface, so its response and recovery time is longer [29].

Discussion

Therefore, the experimental results have shown the sensing performance of SnO$_2$ microfibers assembled by fine nanocrystals sufficiently. First of all, the gas sensors were fabricated by SnO$_2$ hollow microfibers, and the gas molecules could flow through the space between the microfibers due to the loosely stacking, as shown in Fig. 7a. Our previous research has proved that this structure favored the enhancement of gas response of metal oxide materials [1, 18]. Secondly, we will focus on the influence of SnO$_2$ nanocrystals which are elementary units of gas-sensing

Fig. 6 Dependence of the response and recovery time (to 300 ppb formaldehyde at 240 °C) on sintering time

material. It should be noted that their gas response to formaldehyde did not change with the sintering time monotonously; instead it showed an increase firstly and a decrease later. Herein, we will evaluate these two microstructural parameters (surface area and mesopore size) of SnO$_2$ microfibers on gas-sensing properties and dwell upon the reason for this uncommon variation of sensing performance.

It is well known that metal oxide sensing materials with high surface area or reduced grain size may exhibit enhanced sensing performance due to the abundant surface-active reaction sites for gas molecule adsorption and surface reaction [30, 31]. As the grain size of SnO$_2$ reduced to a certain value, which was known as "Debye length" (3 nm for SnO$_2$), SnO$_2$ could exhibit an ultra-high gas response because the grain whose size was below $2L_d = 6$ nm became completely depleted when exposed to air [32]. According to the aforementioned characterizations, Sn2h possessed the highest SSA and smallest grain size, which would provide numerous adsorption and reaction sites for gas-sensing process. Conventionally, these two microstructural properties might imply a relatively high sensing performance.

Surprisingly, in this research an uncommon phenomenon was found that the response of Sn2h was lower than that of Sn6h and Sn11h, and Sn11h exhibited the highest response to ppb-level formaldehyde than other specimens. To investigate the influence of pore diameter and SSA of SnO$_2$ microfibers on their gas response, the dependence of gas response (to 300 ppb formaldehyde at 240 °C), average pore diameter, and SSA on sintering time is depicted and shown in Fig. 7b. This figure demonstrated that the SSA of SnO$_2$ microfibers decreased with increasing sintering time, while the gas response increased gradually. Herein, this result indicated that some other factor dominated their sensing performance in the early stage in which the sintering time is <11 h.

It is worth noting that, besides surface reaction, gas diffusivity also played an important role in influencing the gas-sensing performance. In practical gas-sensing behavior, the individual gas molecule has to reach a certain active region of porous chemiresistive sensing materials through pore or crevice [33]. In this case, the gas molecules diffused into the pores and contributed to a higher gas response because of their concentration gradient in the pores. With regard to these thick-film sensors, whose coating has 50–200 μm depth [34], only the outermost surface of thick-film sensor played a major role in sensing reaction [35]. In this work, the pores in SnO$_2$ microfibers were of typical mesopore, and the transport of gas molecules in mesoporous materials is known as Knudsen diffusion; the diffusion coefficient is given by the equation [36]:
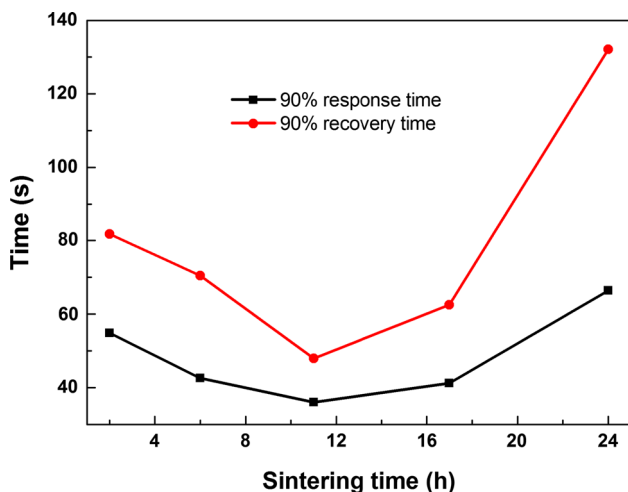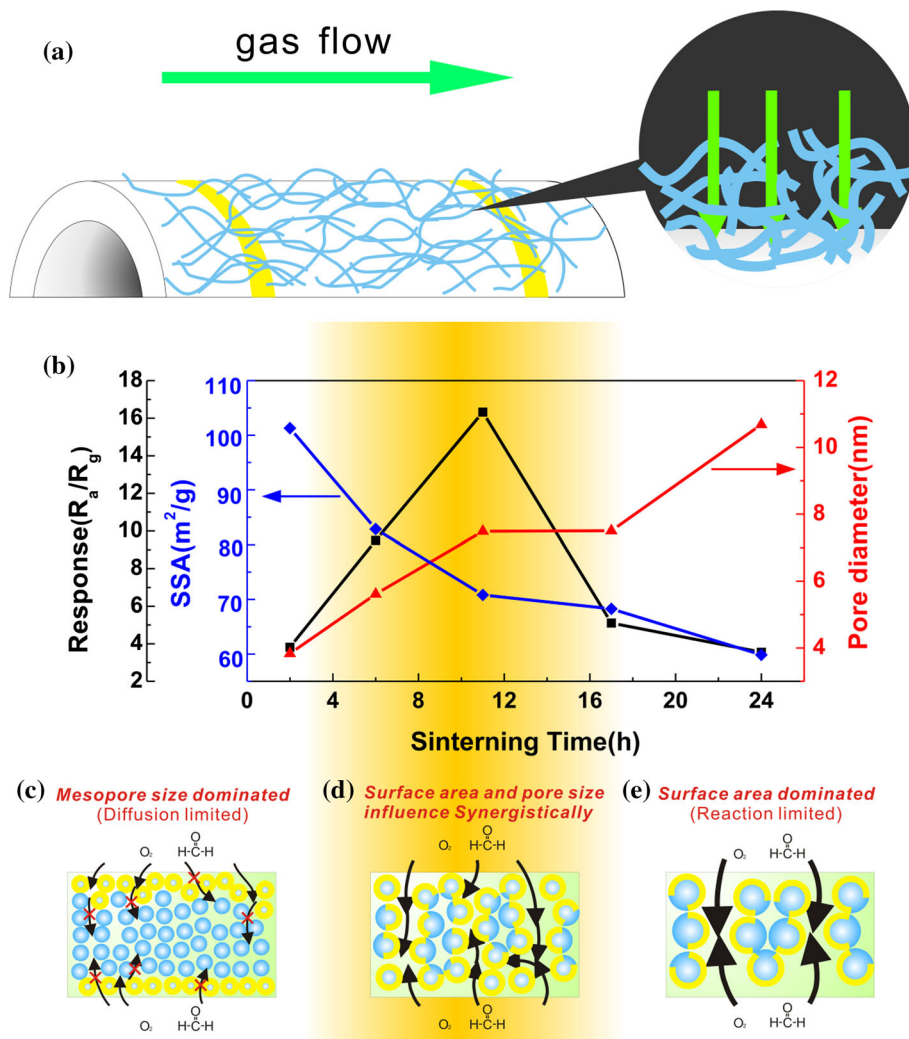
Fig. 7 a Schematic of the SnO$_2$ gas sensor and **b** the dependence of gas response (to 300 ppb formaldehyde at 240 °C), average pore diameter, and SSA on sintering time. **c, d,** and **e** shows gas diffusion models of Sn2h, Sn11h, and Sn24h, respectively

$$D_K = \frac{4r}{3}\sqrt{\frac{2RT}{\pi M}}, \qquad (ii)$$

where D_K is the Knudsen diffusion coefficient, r is the pore radius (cm), T is the temperature (K), R is the universal gas constant and M is the molecular weight of gas (g mol^{-1}). This formula indicated that the gas molecules can diffuse deeper into the sensing layer through the wide open pores and enable the reaction between formaldehyde and oxygen species(O_2^{-}, O^{-}, and O^{2-}) occurring in deeper layer. Sakai successfully built the relationship between sensitivity and gas concentration, and the formula can be expressed as follows [17]:

$$S = 1 + \frac{aC_{A,s}}{L\sqrt{\frac{k}{D_K}}}\tanh L\sqrt{\frac{k}{D_K}}, \qquad (iii)$$

where S is the gas-sensing sensitivity defined as the ratio of R_a to R_g, $C_{A,s}$ is the target gas concentration outside the material, L is the thickness and k is the rate constant. In this formula, gas sensitivity S increased with decreasing m,

namely, the increasing D_K may result in an increase in sensitivity.

Here, the effects of the SSA and pore diameter on sensing performance of SnO$_2$ microfibers were discussed in detail. As shown in Fig. 7c, although Sn2h assembled by fine nanocrystals possessed the highest SSA and smallest grain size, its average pore diameter was 2.8 nm, which was too small to let the gas molecules in. According to the Knudsen diffusion formula, it can be inferred that most of the gas molecules were blocked by the small pores, and thus the diffusion rate was vastly limited. The large amount of the inner channels contributed to the highest SSA value, while they were not accessible for gas molecules in practical gas-sensing process. Therefore, the gas response was only ascribed to the adsorption and reaction on the surface SnO$_2$ nanocrystals of the microfibers, resulting in a lower sensing performance. In this early stage (sintering time <11 h), the pore diameter dominated the gas-sensing performance, rather than surface area. When the sintering time was increased to 11 h, the microstructure of SnO$_2$

fibers changed due to grain growth [37]. The SSA decreased from 103.6 to 70.8 m^2 g^{-1}, while the pore diameter increased from 2.8 to 8.5 nm. As a result, the gas response increased with increasing pore diameter. As shown in Eq. (ii), larger pore diameter meant a higher Knudsen diffusion rate of gas molecules indicating that the outer and inner surface of materials can interact with detected gas molecules, which will be probably increased [17]. As shown in Fig. 7d, the augmented pore diameter enabled more gas molecules to diffuse in and reacted in deeper layer along the wall. It is worth noting that a larger mesopore diameter accelerated the gas transport in the inner of the fibers, and larger SSA ensured the adsorption–desorption and the chemical reaction on the surface of the inner walls [38]. For the same reason, the resistance of Sn11h was larger than that of Sn2h. Therefore, the moderate mesopore diameter and SSA influenced gas-sensing properties synergistically, and Sn11h exhibited the highest gas response to formaldehyde. In the meantime, the shortest response and recovery time to formaldehyde of Sn11h, as shown in Fig. 6, also benefited from the fast diffusion rate and good reaction activity [19]. When the sintering time was increased from 11 to 24 h, despite the increasing pore diameter (increased from 8.5 to 10.9 nm), the gas response decreased drastically, and the schematic model is shown in Fig. 7e. In the late stage (sintering time more than 11 h), the SSA decreased from 70.8 to 59.8 m^2 g^{-1}, which was ascribed to the increasing grain size of SnO$_2$ crystals. As a result, the active adsorption and reaction sites on the surface of SnO$_2$ nanocrystals decreased; in other words, the reaction activity of SnO$_2$ nanocrystals deteriorated [31]. Although the diffusion rate increased to a certain degree, the disadvantages of decreased SSA overwhelmed the positive effects of enlarged mesopore diameter. In addition, the increased response and recovery time was also attributed to the deteriorated surface reaction activity which was closely related to grain size. The smaller grain size provides a more active surface of SnO$_2$ due to the less-coordinated surface Sn atoms [29]; in this sense, the reaction activity of Sn24h was obviously low and its resistance was smaller than Sn11h. Eventually, the gas response of Sn24h decreased and the response and recovery time increased. Thus, the SSA played a dominant role in sensing performance. For mesoporous SnO$_2$ hollow microfibers, surface area and pore diameter were proved to demonstrate their unique effect on the gas-sensing behavior.

To verify the competitive influence of surface area and pore diameter on the sensing performance of mesoporous SnO$_2$ microfibers, we investigated the gas response of the five specimens to hydrogen. Due to its smaller molecular radius and the first-order reaction with oxygen species adsorbed on the surface of metal oxide, hydrogen was
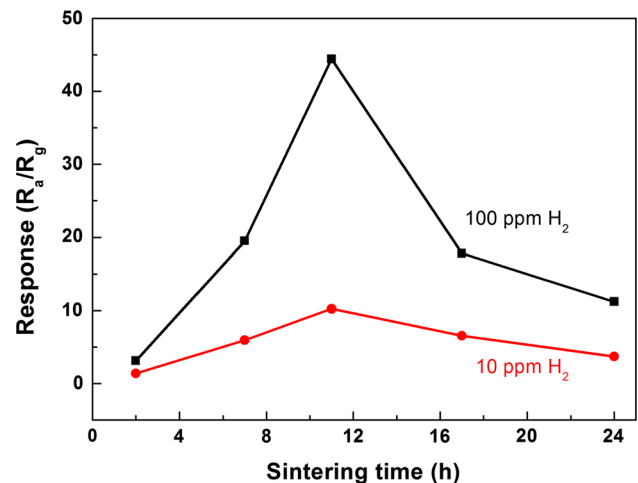

Fig. 8 The response of the five SnO$_2$ specimens to 10 and 100 ppm hydrogen at an operating temperature of 240 °C

suggested to exhibit higher permeability than some other gases [39]. Figure 8 shows their gas response to 10 and 100 ppm hydrogen at 240 °C. This result was consistent with their gas response to formaldehyde, and SnO$_2$ microfibers sintered for 11 h showed the highest response. This result was ascribed to the fact that H$_2$-sensing properties of SnO$_2$-based sensors are determined by the effects of both gas diffusivity and reactivity [40]. It also provided solid evidence that surface area and mesopore size played more significant roles in determining mesoporous gas sensors than molecules' radius. Therefore, the competitive influence of surface area and mesopore size on gas-sensing properties of SnO$_2$ nanocrystals was revealed.

Conclusions

In summary, this work focused on the gas-sensing properties of mesoporous SnO$_2$ hollow microfibers with different sintering times. Their SSA decreased and mesopore diameter increased gradually with increasing sintering time. Interestingly, the gas response increased with the increasing sintering time from 2 to 11 h and then decreased drastically with further increasing sintering time. The mesopore diameter dominated the sensing performance of mesoporous SnO$_2$ microfibers in the early stage of sintering time, while the surface area dominated in the late stage. This result provided solid evidence of competitive influence of surface area and mesopore diameter on the gas-sensing properties of SnO$_2$. This work proposes a new insight into the research on mesoporous metal oxide materials.

References

1. Ding X, Zeng D, Zhang S, Xie C (2011) C-doped WO_3 micro-tubes assembled by nanoparticles with ultrahigh sensitivity to toluene at low operating temperature. Sens Actuators B Chem 155:86–92. doi:10.1016/j.snb.2010.11.030

2. Sarkar S, Basak D (2013) Synthesis of dense intersecting branched tree-like ZnO nanostructures and its superior LPG sensing property. Sens Actuators B Chem 176:374–378. doi:10.1016/j.snb.2012.10.095

3. Wang Y, Jiang X, Xia Y (2003) A solution-phase, precursor route to polycrystalline SnO_2 nanowires that can be used for gas sensing under ambient conditions. J Am Chem Soc 125:16176–16177. doi:10.1021/ja037743f

4. Yi S, Tian S, Zeng D et al (2013) An In_2O_3 nanowire-like network fabricated on coplanar sensor surface by sacrificial CNTs for enhanced gas sensing performance. Sens Actuators B Chem 185:345–353. doi:10.1016/j.snb.2013.05.007

5. Ab Kadir R, Zhang W, Wang Y et al (2015) Anodized nanoporous WO_3 Schottky contact structures for hydrogen and ethanol sensing. J Mater Chem A 3:7994–8001. doi:10.1039/C4TA06286H

6. Chwieroth B, Patton BR, Wang Y (2001) Conduction and gas-surface reaction modeling in metal oxide gas sensors. J Electroceramics 6:27–41

7. Tiemann M (2007) Porous metal oxides as gas sensors. Chem-A Eur J 13:8376–8388. doi:10.1002/chem.200700927

8. Matsunaga N, Sakai G, Shimanoe K, Yamazoe N (2002) Diffusion equation-based study of thin film semiconductor gas sensor-response transient. Sens Actuators B Chem 83:216–221

9. Wu N-L, Tung C-Y (2004) Evolution in microstructural properties of cetyltrimethylammonium bromide-templated mesoporous tin oxide upon thermal crystallization. J Am Ceram Soc 87:1741–1746

10. Landau O, Rothschild A (2012) Microstructure evolution of TiO_2 gas sensors produced by electrospinning. Sens Actuators B Chem 171–172:118–126. doi:10.1016/j.snb.2011.12.061

11. Li L-L, Zhang W-M, Yuan Q et al (2008) Room temperature ionic liquids assisted green synthesis of nanocrystalline porous $SnO2$ and their gas sensor behaviors. Cryst Growth Des 8:4165–4172

12. Korotcenkov G (2005) Gas response control through structural and chemical modification of metal oxide films: state of the art and approaches. Sens Actuators B Chem 107:209–232

13. Li G-J, Kawi S (1998) Synthesis, characterization and sensing application of novel semiconductor oxides. Talanta 45:759–766

14. Yamazoe N (1991) New approaches for improving semiconductor gas sensors. Sens Actuators B Chem 5:7–19

15. Korotcenkov G, Cho BK (2010) Porous semiconductors: advanced material for gas sensor applications. Crit Rev Solid State Mater Sci 35:1–37. doi:10.1080/10408430903245369

16. Melde BJ, Johnson BJ (2010) Mesoporous materials in sensing: morphology and functionality at the meso-interface. Anal Bioanal Chem 398:1565–1573. doi:10.1007/s00216-010-3688-6

17. Sakai G, Matsunaga N, Shimanoe K, Yamazoe N (2001) Theory of gas-diffusion controlled sensitivity for thin film semiconductor gas sensor. Sens Actuators B Chem 80:125–131. doi:10.1016/S0925-4005(01)00890-5

18. Tian S, Ding X, Zeng D et al (2013) Pore-size-dependent sensing property of hierarchical SnO_2 mesoporous microfibers as formaldehyde sensors. Sens Actuators B Chem 186:640–647. doi:10.1016/j.snb.2013.06.073

19. Liu Z, Yamazaki T, Shen Y et al (2007) Influence of annealing on microstructure and NO_2-sensing properties of sputtered WO_3 thin films. Sens Actuators B Chem 128:173–178. doi:10.1016/j.snb.2007.06.001

20. Hyodo T, Nishida N, Shimizu Y, Egashira M (2002) Preparation and gas-sensing properties of thermally stable mesoporous SnO2. Sens Actuators B Chem 83:209–215. doi:10.1016/S0925-4005(01)01042-5

21. Reddy N, Yang Y (2007) Structure and properties of natural cellulose fibers obtained from sorghum leaves and stems. J Agric Food Chem 55:5569–5574. doi:10.1021/jf0707379

22. Cui Z, Liu J, Zeng D et al (2010) Quasi-one-dimensional bismuth tungsten oxide nanostructures templated by cotton fibers. J Am Ceram Soc 93:1479–1483. doi:10.1111/j.1551-2916.2010.03600.x

23. Sathyaseelan B, Senthilnathan K, Alagesan T et al (2010) A study on structural and optical properties of Mn- and Co-doped SnO_2 nanocrystallites. Mater Chem Phys 124:1046–1050. doi:10.1016/j.matchemphys.2010.08.029

24. Huang H, Lee YC, Tan OK et al (2009) High sensitivity SnO_2 single-nanorod sensors for the detection of H_2 gas at low temperature. Nanotechnology 20:115501. doi:10.1088/0957-4484/20/11/115501

25. Kruk M, Jaroniec M (2001) Gas adsorption characterization of ordered organic-inorganic nanocomposite materials. Chem Mater 13:3169–3183

26. Xu C, Tamaki J, Miura N, Yamazoe N (1991) Grain size effects on gas sensitivity of porous SnO_2-based elements. Sens Actuators B Chem 3:147–155

27. Wang D, Hu P, Xu J et al (2009) Fast response chlorine gas sensor based on mesoporous SnO_2. Sens Actuators B Chem 140:383–389. doi:10.1016/j.snb.2009.05.027

28. Korotcenkov G (2008) The role of morphology and crystallographic structure of metal oxides in response of conductometric-type gas sensors. Mater Sci Eng R Rep 61:1–39

29. Ma Y, Qu Y, Zhou W (2013) Surface engineering of one-dimensional tin oxide nanostructures for chemical sensors. Microchim Acta 180:1181–1200. doi:10.1007/s00604-013-1048-x

30. Li G-J, Zhang X-H, Kawi S (1999) Relationships between sensitivity, catalytic activity, and surface areas of SnO_2 gas sensors. Sens Actuators B Chem 60:64–70

31. Baraton M-I, Merhari L (2001) Influence of the particle size on the surface reactivity and gas sensing properties of SnO_2 nanopowders. Mater Trans 42:1616–1622

32. Franke ME, Koplin TJ, Simon U (2006) Metal and metal oxide nanoparticles in chemiresistors: does the nanoscale matter? Small 2:36–50. doi:10.1002/smll.200500261

33. Wagner T, Haffer S, Weinberger C et al (2013) Mesoporous materials as gas sensors. Chem Soc Rev 42:4036. doi:10.1039/c2cs35379b

34. Korotcenkov G (2007) Practical aspects in design of one-electrode semiconductor gas sensors: Status report. Sens Actuators B Chem 121:664–678. doi:10.1016/j.snb.2006.04.092

35. Rani RA, Zoolfakar AS, Ou JZ et al (2013) Nanoporous Nb2O5 hydrogen gas sensor. Sens Actuators B Chem 176:149–156. doi:10.1016/j.snb.2012.09.028

36. Shimizu Y, Jono A, Hyodo T, Egashira M (2005) Preparation of large mesoporous SnO_2 powder for gas sensor application. Sens Actuators B Chem 108:56–61. doi:10.1016/j.snb.2004.10.047

37. Shek CH, Lai JKL, Lin GM (1999) Grain growth in nanocrystalline SnO_2 prepared by sol-gel route. Nanostructured Mater 11:887–893

38. Seo M-H, Yuasa M, Kida T et al (2009) Gas sensing characteristics and porosity control of nanostructured films composed of TiO$_2$ nanotubes. Sens Actuators B Chem 137:513–520. doi:10.1016/j.snb.2009.01.057

39. Kida T, Fujiyama S, Suematsu K et al (2013) Pore and particle size control of gas sensing films using SnO2 nanoparticles synthesized by seed-mediated growth: design of highly sensitive gas sensors. J Phys Chem C 117:17574–17582. doi:10.1021/jp4045226

40. Shimizu Y, Maekawa T, Nakamura Y, Egashira M (1998) Effects of gas diffusivity and reactivity on sensing properties of thick film SnO2-based sensors. Sens Actuators B Chem 46:163–168. doi:10.1016/S0925-4005(97)00247-5